6-2014

2014 SAE Aero: Systems Engineering

Adam Herzog
Union College - Schenectady, NY

2014 SAE Aero Competition:

Systems Engineering

By

Adam Herzog

* * * * * * * * *

Submitted in partial fulfillment

of the requirements for

Honors in the Department of Mechanical Engineering

UNION COLLEGE

June, 2014

ABSTRACT

HERZOG, ADAM 2014 SAE Aero Competition: Systems Engineering. Department of Mechanical Engineering, June 2014.

ADVISOR: [Professor Bradford Bruno PH.D.]

Union has participated in the annual SAE Aero Competition for the last 6 consecutive years. The aim of the competition involves the design and construction of an RC aircraft capable of carrying a maximum payload weight as consistently as possible. This report will summarize the methods used to determine shape and size of the final aircraft's control surfaces, as well as include an analysis on the plane's performance characteristics. The final design utilizes a 100 inch span main wing with a rear taper and an upright H-tail design. In addition, the horizontal tail has a stabilator in place of a horizontal stabilizer with elevators. This configuration was found to minimize the effects of drag and maximize performance at the anticipated Reynolds Number the plane will be flying at. Previous design iterations were proven to be inefficient after the completion of a to-scale working prototype in the middle of the project's design process. A theoretical estimate of this plane's maximum takeoff weight was calculated to be around 30 lbs., taking into account a 200 ft. runway with the effects of variable thrust and drag. The plane will be competing April 11-13, 2014 in Marietta, GA.

TABLE OF CONTENTS:

1.0: INTRODUCTION

This document describes the final aircraft design and design process from the perspective of a systems engineer for participation in the 2014 Society of Automotive Engineers (SAE) Aero Design East Competition – Regular Class. The competition is meant to provide engineering students a level of exposure to the situations and challenges that practicing engineers will face in a realistic work environment.

There are three different classes of competition; the advanced class, the regular class, and the micro class. Historically, Union has participated in the regular class competition and will continue to do so this year. The micro class, as its name suggests, calls for the design of a small, electrically powered aircraft, capable of fitting within a specifically sized travel case. If future teams acquire more student involvement, this micro class might be an option for juniors or sophomores to get involved. The advanced class involves the construction of a larger airplane than that of the regular class. The objective allows for its construction to utilize composite materials and requires the plane to drop a care package on a target from a pre-defined altitude. The complexity of this class is not realistic for Union's current team of four and would benefit from the assistance of an electrical engineer.

The Regular Class of competition, which Union's current SAE Aero team will be competing in, involves the design and construction of an aircraft capable of carrying a maximum payload weight and maintaining stable flight. Scoring for

this year's competition is comprised of a technical paper score, presentation score, and an overall flight score.

The rules and regulations for this year's competition have undergone four main changes: the alteration of the permitted propulsion mechanism, the size limitations, the payload housing, and the competition scoring. Any type of electric motor, drawing no more than 1000 Watts is now required for the propulsion mechanism versus the gas-powered engine used during previous competitions. The size limitations for this year's regular class were reduced from 225 inches to 175 inches, resulting in a smaller final design. The payload housing/integration system must now take the form of a 4" x 4" x 10" rectangular prism and the competition scoring has now been modified to sum the results of all flights as opposed to previous years that used the best scored flight[7].

2.0: DESIGN PROCESS

The following section will describe and outline the design approach and progression of the airfoil selection, wing design, tail design, and design review process. The final aircraft configuration of Union College's SAE Aero team is shown in Figure 1.

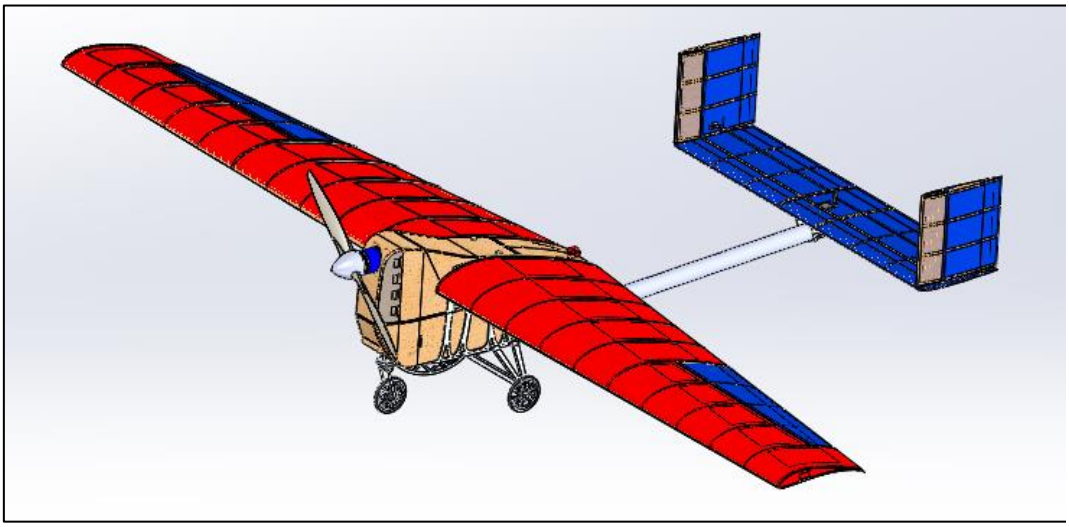

Figure 1: *Union's final design for the 2014 SAE Aero Design Competition*

2.1: AIRFOIL SELECTION

Airfoils generate lift by creating pressure differences between their lower and upper surfaces, separated by a stagnation point in the airflow at the leading edge and a convergence of airflow at the trailing edge. As air travels over the upper surface, it increases velocity and decreases in pressure. Conversely, as air travels under the wing, its velocity deceases and increases in pressure. These pressure differences create a lifting force that makes flight possible.

Due to the nature of this competition and its design objective, a high lift, low airspeed airfoil shape was desired. Basic characteristics of these airfoils are

relatively thick leading edges, high camber (or curvature), high drag coefficients, and larger pitching moments than a symmetrical airfoil.

Teams from previous years performed extensive research to determine the most efficient shape for this high lift, low airspeed application. Their decision on airfoil selection was the Selig S1223 shape, shown below in Figure 2.

Figure 2: *The Selig S1223 airfoil shape that was chosen and implemented in the design of the main wing* [11]

Research indicated that a potential alternative to this selection was the E423 airfoil shape. Although both the S1223 and E423 airfoil shapes are designed for high lift, low speed flight, the S1223 was the best decision for a wing with a high angle of incidence. The lift coefficient curve for the E423 airfoil exhibited higher lift at lower angles of attack with a lower maximum lift coefficient than that of the S1223. Practical use of the E423 airfoil would require a lower angle of incidence with more thrust than this year's plane is capable of producing.

Before any of the performance calculations could be completed, it was necessary to determine the anticipated Reynolds number that the plane would be flying at. The Reynolds number (Re) is a dimensionless number used to relate inertial forces to viscous forces. Equation 1 shown below was used to determine Re where ρ is the air density, v is the airspeed of the plane, $\bar{c}$ is the mean aerodynamic chord (MAC, explained later), and μ is the dynamic viscosity of the air.

$$Re = \frac{\rho v \bar{c}}{\mu} \quad (1)$$

Values of air density and dynamic viscosity were estimated using the average temperature and pressure of Marietta, GA, where the competition will be held. The velocity and chord length were estimated from the previous year's performance, keeping in mind that this year's plane will be smaller and have slightly less thrust.

After determining that this year's plane will be flying at an anticipated Reynolds number of approximately 250,000, the lift and drag coefficient curves for the S1223 airfoil shape were found. Previously tabulated values for the lift coefficient (C_L), coefficient of moment (C_m), and drag coefficient (C_D) versus the angle of attack (α) for the S1223 airfoil are shown below in Figure 3.

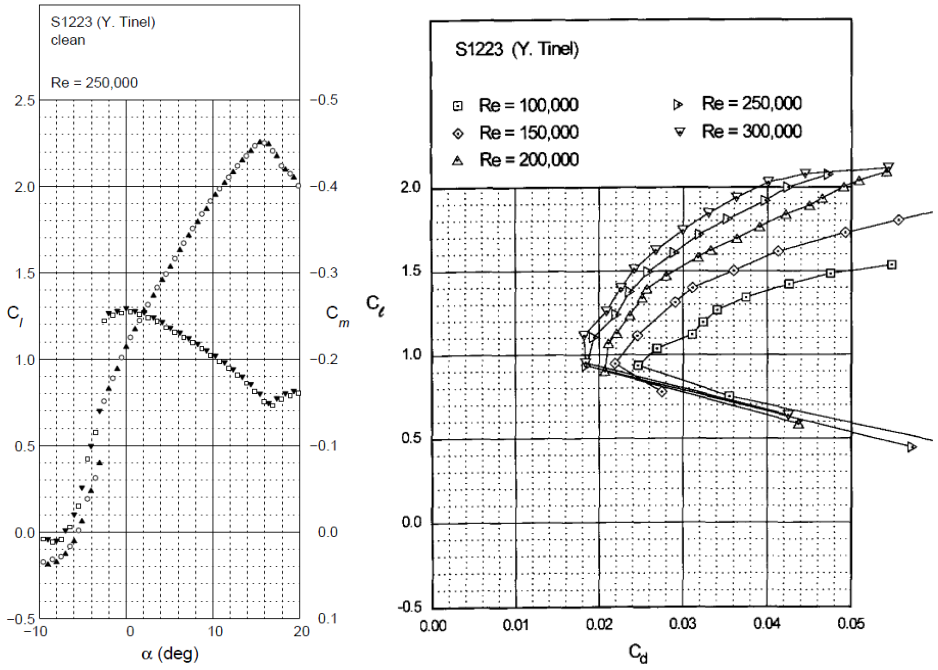

Figure 3: *The lift and moment coefficient curves (left) and the drag coefficient curve (right) for the Selig S1223 airfoil shape* [11]

Likewise, the selection process for the tail's airfoil shape was guided by the previous year's selection. Following the convention of a symmetric airfoil, the NACA 009 airfoil was chosen. This airfoil shape provided minimal drag with enough space in the horizontal stabilizer for adequate structural support. The lift and drag coefficient curves for the NACA 009 airfoil can be viewed below in Figure 4.

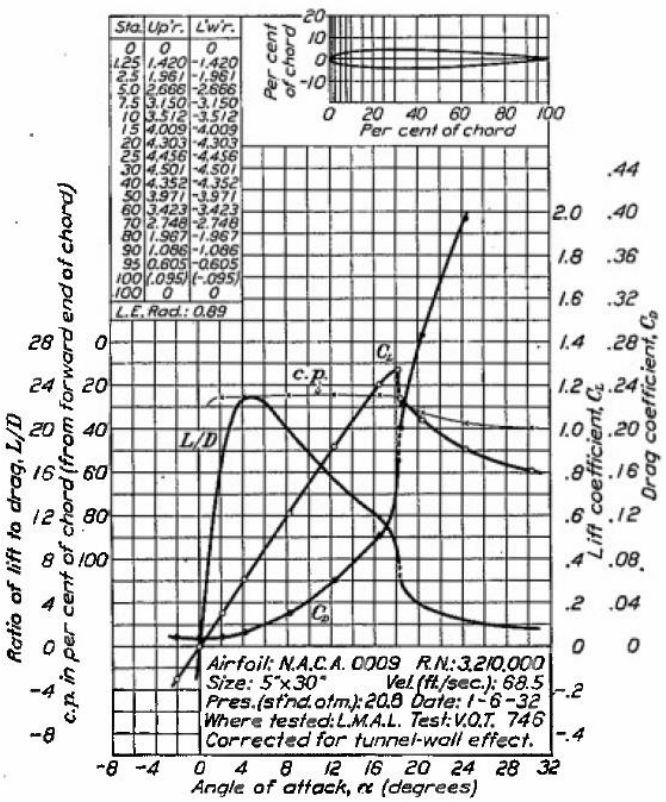

Figure 4: *The lift and drag coefficient curves for the NACA 009 airfoil shape* [3]

2.2: WING DESIGN

The first priority in wing design was to determine the appropriate planform or shape. Previous year's teams have been slowly working towards a full taper design to reduce the effects of lift induced drag. Induced drag is caused by flow

vortices that form at the wing tips due to the three-dimensional lift distribution over the wing surface. Theoretically, a wing with an infinitely long span would experience zero induced drag because there are no wing tips. The effect of induced drag at low airspeeds is significant relative to the overall drag. Calculations have confirmed that approximately 80% of the total drag on the final aircraft's wing is due to these tip vortices.

The most efficient wing shape for eliminating the effects of induced drag is an ellipse. The lift distribution over an ideally shaped elliptical wing would look as shown in Figure 5. However, an elliptical design was too difficult to manufacture. The main spar for an elliptical wing would need to pass through the center of the wing where the thickness of the airfoils is too thin and the exterior surface would not be able to adhere to the wing without creating wrinkles. Figure 6 below illustrates the different designs that were considered during the design process.

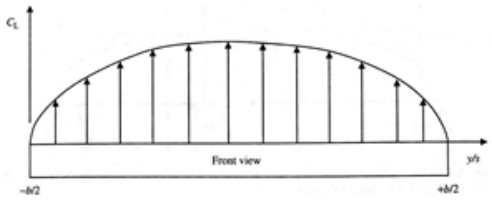

Figure 5: *The lift distribution over an ideally shaped elliptical wing, neglecting interference from the fuselage* [6]

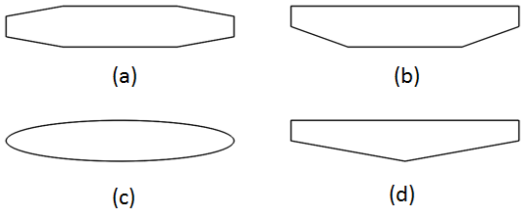

Figure 6: *The different wing shapes that were considered during the design process*

It is for this reason that a high emphasis was placed on a tapered wing rather than a wing with constant chord length. This year's design used a planform following shape (d) in Figure 6. Wings (a) and (c) were both too difficult to construct and internally support while research indicated that a planform

following wing shape (b) would have produced more drag than a planform utilizing shape (d).

The longitudinal location of the wing relative to the fuselage was chosen to maximize the lateral stability of the plane. This led to a high wing design to keep the center of gravity (CG) below the wing during flight. Section 3.2 later on will further discuss the analysis of the aircraft's stability.

The process of sizing the tail and main wing with the rest of the plane was an iterative progression. Maintaining a competitive design that utilized the available space required constant observation of the dimensional limits. After many different widths (correlating to the span of the main wing) were chosen and checked against the size limitation, a final length of 57 inches and height of 17 inches was selected. These values, when added to the 100 inch wingspan, left 1 inch of length before passing over the length plus width plus height dimensional limit. The length and height of the plane can be viewed in Figure 7 below using the final landing gear and tail/tail boom designs. Additionally, using an angle of incidence of 7^0 with a main wing that reaches its maximum lift coefficient at 16^0, the maximum allowable takeoff angle of 10^0 provided just enough ground clearance for proper take-off.

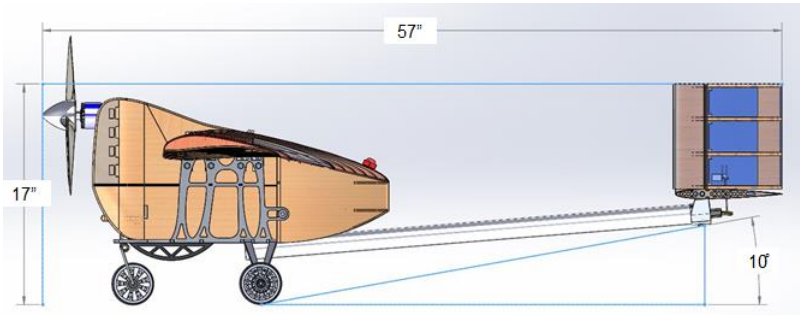

Figure 7: *The 2-dimensional configuration of the aircraft; used to help ensure that the length plus width plus height measurement remained below 175 inches*

As mentioned previously, the main objective behind the design of the main wing's shape was to reduce the effects of induced drag. The induced drag coefficient ($C_{D,i}$), calculated with equation 2 below, is a function of the instantaneous lift coefficient (C_L), the aspect ratio (AR), and the Oswald efficiency factor (e).

$$C_{D,i} = \frac{C_{L,w}^2}{\pi e(AR)} \tag{2}$$

Given the fixed span of 100 in. and a full taper design with a straight leading edge, research indicated that a taper ratio of 0.5 would maximize the Oswald efficiency factor of the wing to an estimated value of 0.85[19]. Equation 3 relates the taper ratio (TR) to the tip (c_{tip}) and root chord (c_{root}) of the main wing.

$$TR = \lambda = \frac{c_{tip}}{c_{root}} \tag{3}$$

The aspect ratio, calculated in equation 3 (where b_w is the wingspan), is inversely proportional to the induced drag coefficient and the area of the wing (A_w).

$$AR = \frac{b_w^2}{A_w} \tag{3}$$

Consider the following: The larger the aspect ratio, the smaller the induced drag and the faster the aircraft can travel. A wing with excessive surface area will have a significant amount of drag, limiting the achievable velocity of the plane. Keeping this in mind, there is an optimal relationship between aspect ratio and wing area which will lead to an ideal chord length. After multiple design iterations,

a root chord of 18 in. was selected to keep both the wing area and aspect ratio at high values. This resulted in corresponding values of 1350 in^2 and 7.14 respectively, shown in Figure 8 below.

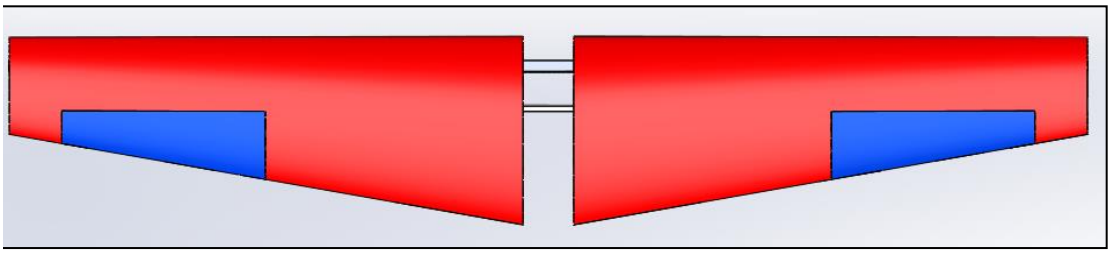

Figure 8: *The final design of the main wing*

2.3: TAIL DESIGN

A plane has three rotational degrees of freedom (DOFs) while in flight. Figure 9 below illustrates these characteristic DOFs. The tail is responsible for controlling pitch with the elevators and yaw with the rudders while roll is controlled with the ailerons on the outer areas of the main wing.

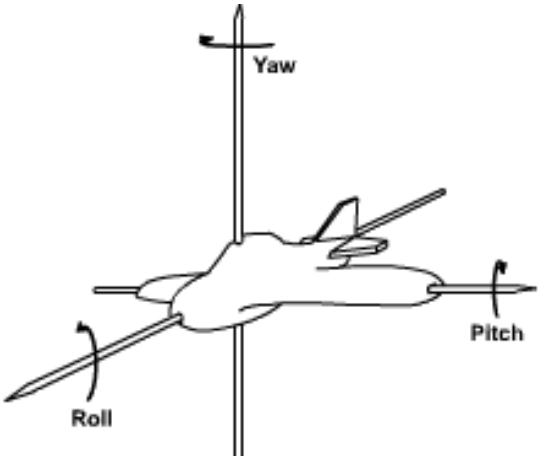

Figure 9: *The three rotational freedoms; pitch, yaw, and roll, of any aircraft* [14]

The inverted tri-tail design, similar to an inverted version of image (h) in Figure 10, of last year's aircraft was necessary to control steering on the runway. At

lower speeds during take-off the central rudder behind the wash of the propeller gave control while the outer rudders did not have enough authority to maneuver the plane. This year's design uses a similar upright H-Tail design, similar to image (d) in Figure 10, without the need for the central rudder because of the addition of a steerable landing gear.

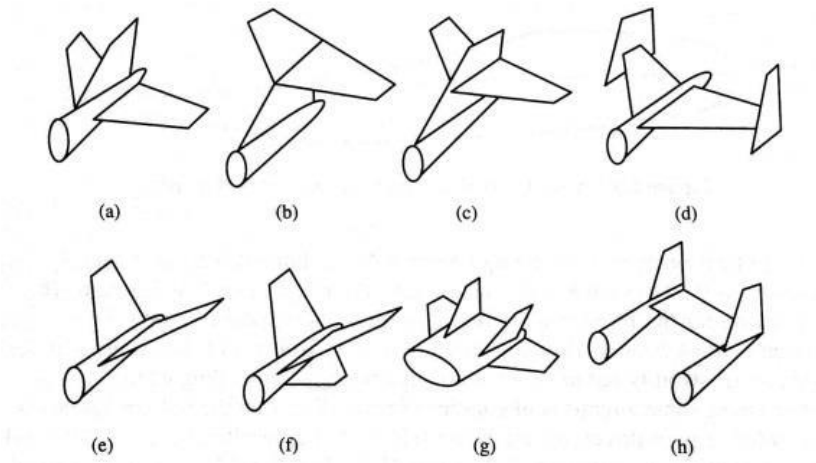

Figure 10*: Common tail designs of traditional aircrafts. The H-Tail design used by last year's team is represented most closely by image (h). This year's design was focused closely around (d)* [6]

A large problem encountered in last year's design was the weight build-up of the servos in the tail. The tail's heavy weight, combined with its large moment arm to the plane's center of gravity, caused the need for 12 lbs. of ballast weight positioned in the nose of the plane to allow for empty flights. Design changes of this year's plane reduced the number of servos in the tail from five to two. One servo is located in the horizontal stabilizer to control the rudders while a second servo is at the aft end of the tail boom to control the pitch of the stabilator (stabilator defined in the next paragraph). This resulted in a significant reduction of weight in the tail.

A traditional airplane uses elevators to control the pitch. Union College's design for this year's plane will feature a stabilator as an alternative. A stabilator, or "full moving tail," combines the function of the horizontal stabilizer with the elevators. Designed to rotate about its aerodynamic center (AC), there are smaller pitching moments involved with a stabilator. The AC is the location along an airfoil where the pitching moment is constant regardless of angle of attack ($\partial C_L/\partial \alpha = 0$). This allows a reduction in the amount of structural support and the number of servos required in the tail, ultimately reducing its weight. Initially, the distance between the main wing and the tail was proportionally decreased from that of last year's plane to abide by the reduction in size limitation. An appropriate design change for this year's plane involved decreasing the span of the main wing to allow for a greater distance between the center of gravity and the tail. This allowed for a slightly lighter tail/tail boom assembly that will provide much more pitch and yaw control for the pilot. A cross sectional view of the stabilator mechanism can be seen in Figure 11 below.

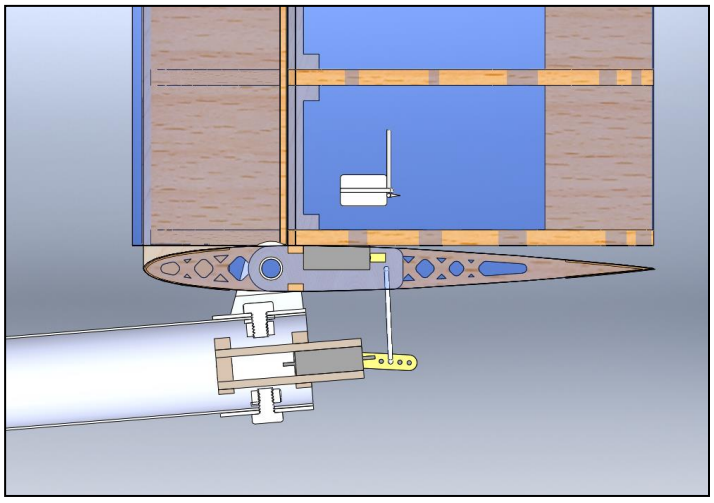

***Figure 11**: A cross sectional view of the stabilator mechanism. The horizontal stabilizer will pivot about the AC of the airfoil.*

An area of concern throughout the conceptualization process was whether or not deep stall would occur. Deep stall occurs when the elevator passes through the wash of the main wing, resulting in a loss of pitch control. It is imperative that deep stall and stall of the main wing do not occur at the same instant. Last year's approach to avoiding deep stall was accomplished by ensuring that the tail remains above the wash of the main wing at all flight positions. This year's design ensures the opposite. The stabilator will always remain below the wash of the main wing. This design strategy used less overall distance in the aircraft's height dimension, allowing more distance for the length and width dimensions.

The process of sizing the tail utilized the tail volume coefficient method of Daniel Raymer[5]. This method uses sizing coefficients of traditionally successful aircrafts to determine an acceptable surface area for the vertical and horizontal surfaces. Equations 4 and 5 were used for the horizontal and vertical tails, respectively, with a horizontal tail sizing coefficient (C_{HS}) of 0.55 and a vertical tail sizing coefficient (C_{VS}) of 0.038. Other variables such as the area of the main wing (A_w), and the distances between the AC of the main wing and the AC's of the horizontal and vertical tails (L_{HS} and L_{VS}) were used to find the required areas of the tail surfaces.

$$A_{horizontal} = C_{HS}\frac{\bar{c}A_w}{L_{HS}} \tag{4}$$

$$A_{vertical} = C_{VS}\frac{\bar{c}A_w}{L_{VS}} \tag{5}$$

The mean aerodynamic chord (MAC or $\bar{c}$) is important in aerodynamic analysis to determine the location of the AC. Using equation 6 below, the MAC of the final wing was calculated to be 14 inches.

$$MAC = \bar{c} = c_{root}\frac{2}{3}\left(\frac{1+\lambda+\lambda^2}{1+\lambda}\right) \quad (6)$$

The AC of the wing is located approximately 25% of the MAC (3.5 inches) aft of the leading edge. It is at this specific point that the pitching moment of the wing does not change with the angle of attack.

Returning to the sizing of the tail surfaces, a moment arm of 38.5 in. and chord lengths of 8.2 in. were chosen for both the vertical and horizontal tail surfaces. This insured that the dimensional requirements were satisfied. These dimensions led to a final aircraft configuration with a horizontal tail area of 270 in^2 and a vertical tail area of 133 in^2, shown in Figure 12 below.

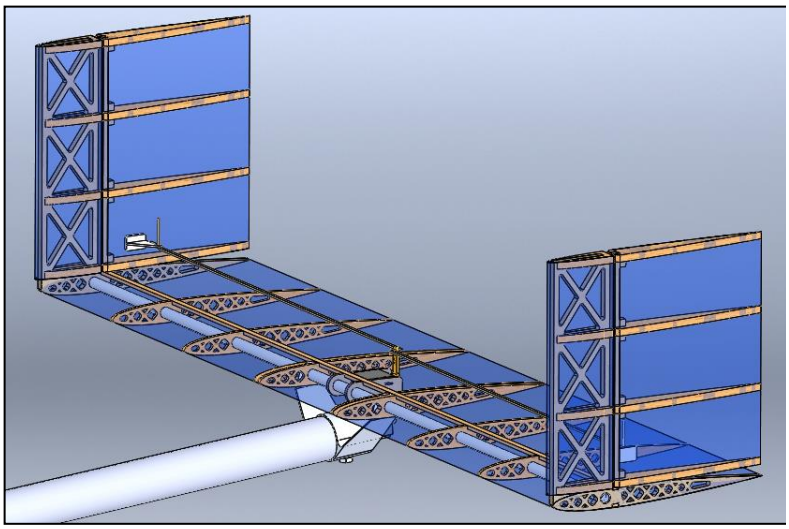

***Figure 12**: The final tail design*

2.4: DESIGN REVIEW PROCESS

The most significant part of the review process for the aircraft was the construction and test flight of a prototype in January. Initially a 110 inch wingspan was used in the design; however, after constructing the prototype it was realized that the plane had surpassed the dimensional limitations by just over 10 inches. A computer generated rendering of the prototype alongside the final construction can be viewed in Figure 13 below. The prototype featured a double tail boom assembly, similar to that of last year's plane with the tail booms connecting to the outer ends of the fuselage. Additionally, the issue of deep stall was addressed in the same way that last year's design had done. The tail was placed above the wing where it would not pass through the wash.

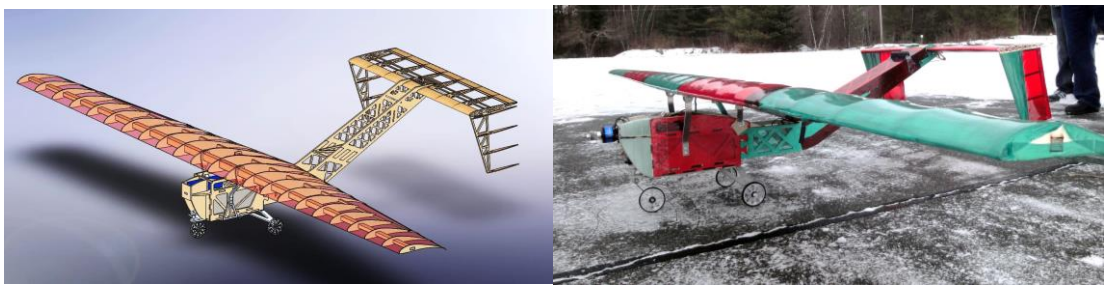

***Figure 13**: A computer generated model of the prototype aircraft (left) above its final construction (right)*

In response to failing to meet the dimensional limitations, the wing was reduced in span, while the tail was lowered and inverted from the prototype's design. The double tail boom was replaced with an aluminum tube tail boom for multiple reasons. After moving the tail to a lower position, the unusual shape of the tail boom shown in Figure 13, previously needed to prevent the boom from passing through the wing, was no longer needed. The aluminum tail boom proved to be stronger, simpler, and lighter than that of the wooden tail boom.

The prototype never successfully flew during testing. This is due to an issue, discussed later in Section 3.2, which prevented the plane from successfully taking off. The rear landing gear was located too far aft, preventing the plane from being able to pitch upwards and take off. The discovery of this issue led to an appropriate design change that shifted the landing gear further forward. Separate modifications in the final design from the prototype included the following: Connecting the fuselage directly into the wing to improve structural rigidity and designing an aluminum skeleton for the fuselage that is directly welded to the landing gear.

3.0: AERODYNAMIC PERFORMANCE

Estimates for the final take-off speed and maximum payload prediction were calculated to determine the plane's performance at competition. Additionally, forward and aft limitations for the location of the CG were established in order to ensure the longitudinal stability of the plane. The following sections will discuss the methods for finding these key performance parameters.

3.1: PAYLOAD AND VELOCITY ESTIMATION

A major rule stated by SAE for the competition requires that no aircraft can travel more than 200 feet down the runway before the landing gear lifts off the ground. The relationship between the velocity of the plane and the distance it travels is more complicated than one would initially think. The maximum allowable payload weight was calculated by mathematically relating lift, gravity, drag, thrust, and the inertial forces acting on the aircraft to eventually solve for the plane's mass. Equations 7 and 8 were used as the basis for finding this mathematical relation where v is the plane's instantaneous velocity, s is the distance from the starting point along the runway, t is the time from leaving the starting point, and a is the plane's instantaneous acceleration.

$$v = ds/dt \tag{7}$$

$$a = dv/dt \tag{8}$$

Along with Newton's Second Law, these equations can be substituted into one another to give equation 9 where s_f is the end of the runway at 200 feet, v_f

is the unknown final velocity of the plane at take-off, m is the plane's maximum allowable mass, and F_{net} is the net force acting on the plane.

$$ads = vdv \Rightarrow \int_0^{s_f} ads = \int_0^{v_f} vdv \Rightarrow \qquad \frac{s_f}{m} = \int_0^{v_f} \frac{v}{F_{net}} dv \tag{9}$$

The net force acting on the plane consists of four main component forces. These forces include the drag force, thrust force, lift force, and gravitational force (i.e. the weight). At takeoff, the weight and lift force are equal to one another. Equation 10 below was used to calculate the lift (L) of the main wing where $C_{L,w}$ is the lift coefficient at the plane's takeoff angle of attack of 16^0. Solving for the final velocity of the plane at take-off with this relation gives equation 11, later used for the upper limit of the velocity integral in equation 9.

$$L = \frac{1}{2}\rho v^2 C_{L,w} A_w \tag{10}$$

$$v_f = \sqrt{\frac{2mg}{\rho C_{L,w} A_w}} \tag{11}$$

The drag force (D) on the plane comes from drag on the main wing, the tail, and the fuselage, calculated the same way that the lift force is in equation 10 using a drag coefficient rather than a lift coefficient. The main wing has the additional effect of induced drag; however, the overall drag can be found in terms of the velocity, for use in equation 9, using equation 12 below. It should be noted that the subscripts "s" and "f" denote the tail (or stabilator) and fuselage respectively in this equation. The drag coefficient used for the fuselage corresponds to that of a rectangular flat plate with the same frontal area. This

was done for the purpose of over-estimating the total drag and finding a conservative allowable payload.

$$D = \frac{1}{2}\rho v^2 \left[\left(C_{D,w} + \frac{C_{L,w}^2}{\pi e (AR)} \right) A_w + C_{D,s} A_s + C_{D,f} A_f \right] \quad (12)$$

The drag force increases with velocity while the thrust force decreases. It is for this reason that the plane will stop accelerating at a certain velocity, where the thrust force and drag force are in equilibrium. The dynamic thrust of the propeller (T) can be calculated in terms of a thrust coefficient (C_T), the air density, and the propeller's diameter (D_p), RPMs (n_p), and efficiency (η_p) in equation 13 below.

$$T = \eta_p C_T \rho n_p^2 D_p^4 \quad (13)$$

The thrust coefficient for the 18x8E propeller used in the final design is plotted against the advance ratio (J), calculated with equation 14 and shown in Figure 14 below.

$$J = \frac{v}{n_p D_p} \quad (14)$$

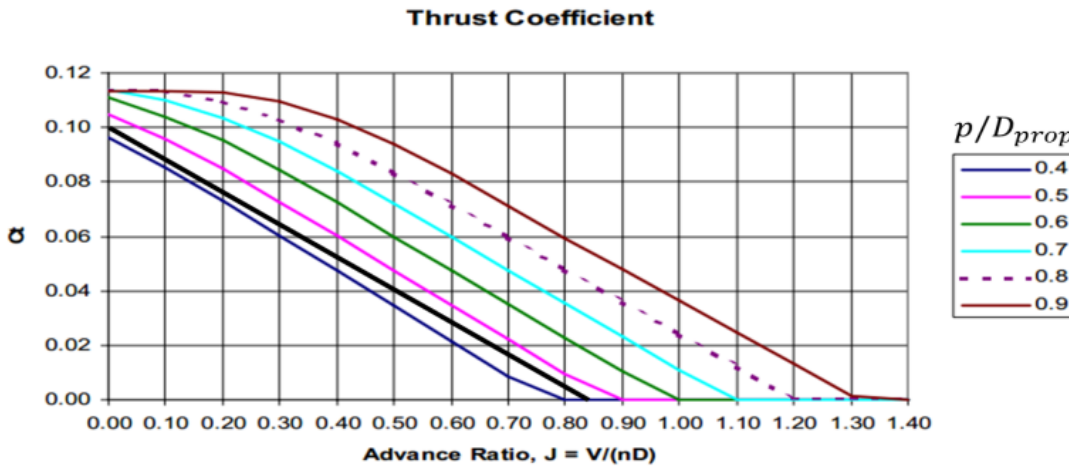

***Figure 14**: A plot of the advance ratio versus the thrust coefficient. A straight line approximation for the 18x8E propeller is indicated by the thick black line.* [2]

Using a straight line approximation for the relationship between thrust coefficient and advance ratio, the thrust was re-written in terms of the velocity in equation 15. The propeller efficiency was determined using this relationship and the experimental data (a thrust of 8.7 lbs. at an advance ratio of zero).

$$T = \eta_p \left(0.10 - 0.1185 \frac{v}{n_p D_p}\right) \rho n_p^2 D_p^4 \tag{15}$$

Once the drag and thrust were found in terms of the plane's velocity, the difference between the two opposing forces was defined as the net force acting on the plane. After substituting equations 11, 12, and 13 into equation 9, the only unknown value left was the maximum allowable mass. Since this function would be exceedingly difficult to integrate by hand, the maximum allowable mass was numerically solved for using Mathematica®, a computational software program. Once the mass was found, the corresponding takeoff velocity was found by re-using equation 11. Final values of the allowable payload versus density altitude, corresponding to the final aircraft weight of 11.2 lbs., are shown in Figure 15 on the next page. The approximate takeoff speed is estimated to be about 35 feet/sec.

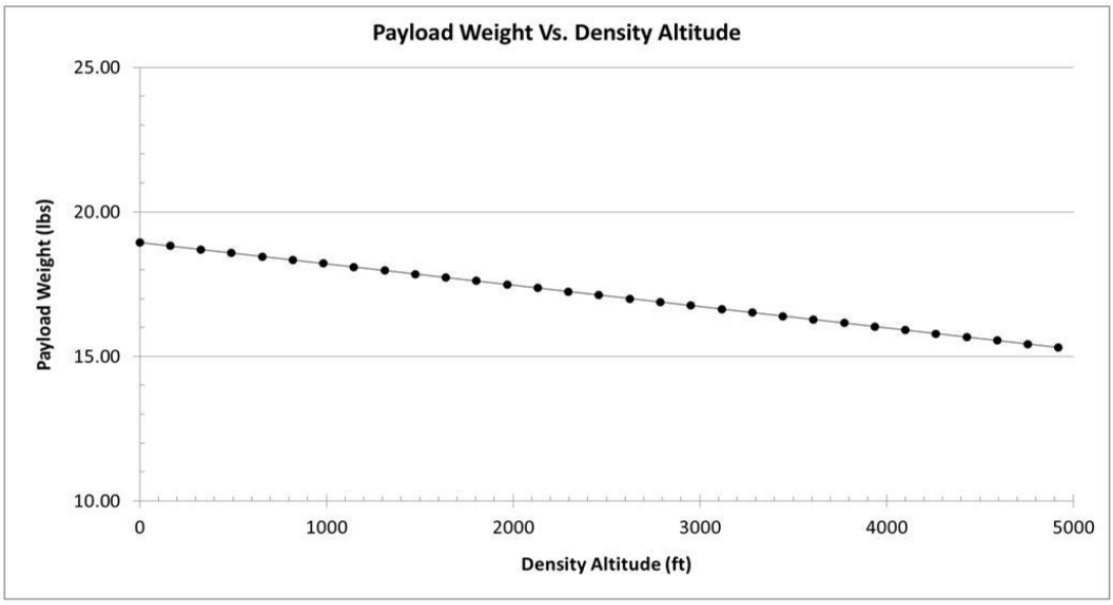

$$W_{\max} = 18.9 - (7 \times 10^{-4}) h_{\text{Density}}$$

***Figure 15**: A plot of the allowable payload weight versus density altitude with the corresponding linear equation*

3.2: LONGITUDINAL STABILITY

The stability of the plane mainly depends on the longitudinal static stability and the longitudinal dynamic stability. Static longitudinal stability is the tendency of the plane to instantaneously return to equilibrium after a disturbance in the pitching plane. The dynamic longitudinal stability is a measurement of how capable the plane is able to return to equilibrium in the pitching plane over time. Figure 16 illustrates the different possibilities of longitudinal stability.

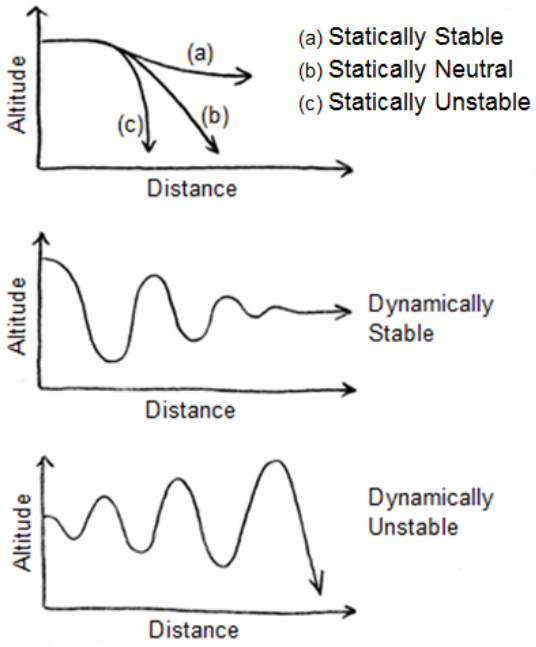

***Figure 16**: Flight behavior associated with different static and dynamic longitudinal stability characteristics* [17]

The static longitudinal stability is directly affected by the location of the aircraft's CG. A CG located as far forward as possible will ensure static longitudinal stability. However, without a large enough tail an aircraft with a far forward placed CG will experience one of two failure modes. Upon takeoff, the tail could potentially not have enough authority to lift the nose off of the ground. This is the issue that was experienced with the prototype mentioned earlier. Alternatively, once in flight, the plane has the potential to lose pitch control and nose dive into a crash. Analysis of these failure modes was accomplished by performing a force and moment balance on the aircraft. Moments were summed about the AC of the wing (analyzing for the in-flight failure mode) and the rear landing gear (for the takeoff failure mode). Both methods were performed with

the CG at its forward limit and the horizontal tail at its maximum downward deflection angle.

Figure 17 below displays the free body diagram used to perform the force and moment balance explained in the paragraph above. All lift forces, drag forces, and pitching moments correspond to the aircraft's geometry at an airspeed of 35 feet/sec. This airspeed was estimated using the takeoff velocity function mentioned in Section 3.1 with the tail at its maximum downward deflection angle.

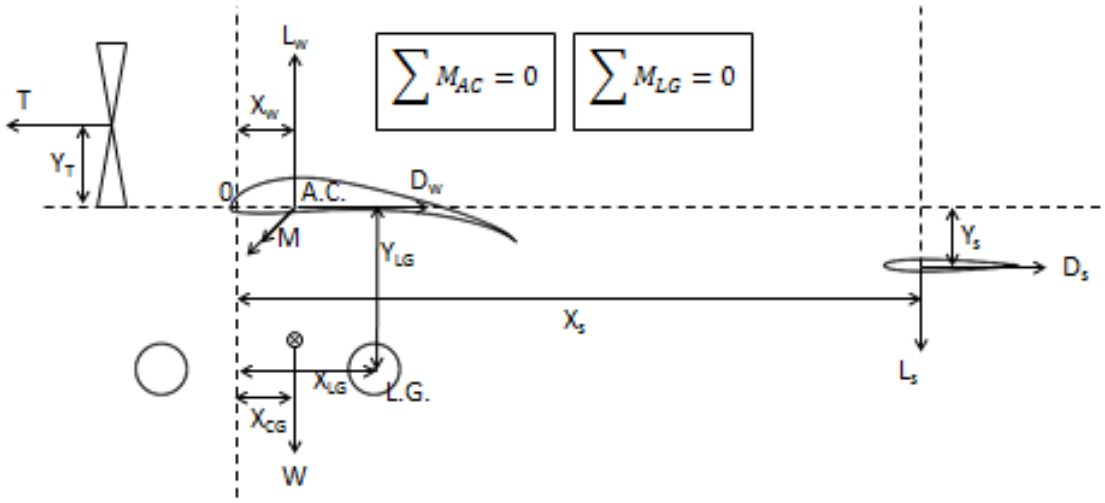

Figure 17: *The free body diagram of the plane with all aerodynamic forces acting on their respective control surfaces*

Finding the forward CG limit of the plane using the free body diagram in Figure 13 consisted of two different calculations. These two calculations involved summing and setting equal to zero all of the moments about both the AC of the main wing and the rear landing gear. Summing the moments about the rear landing gear determined the forward limit of the CG that allows the plane to perform a normal takeoff. If the CG exceeds this limit the plane cannot takeoff. The same process was performed at the AC location on the main wing. This

determined the forward limit that the CG could be placed to keep the plane from experiencing an unrecoverable downward pitch.

Equation 16 was used to determine the forward CG limit during takeoff. Lift and drag forces correspond to the aircraft's 7° angle of incidence.

$$x_{CG} = \frac{1}{W}\left[M + T(y_T + y_{LG}) + W x_{LG} - L_w(x_{LG} - x_w) - D_w y_{LG} - L_s(x_s - x_{LG}) - D_s(y_{LG} - y_{s)}\right] \quad (16)$$

Alternatively, equation 17 was used to determine the forward CG limit of the aircraft in flight.

$$x_{CG} = \frac{1}{W}[T y_T + M + W x_w - L_s(x_s - x_w) + D_s y_s] \quad (17)$$

With these two failure modes, the forward CG limit of the aircraft was determined for all possible masses.

When analyzing how far aft the CG can be placed while maintaining static longitudinal stability, the farthest aft that the CG can be placed is at the "neutral point". The neutral point is defined as the CG location that will result in a statically neutral aircraft. If the CG is located behind the neutral point, the aircraft will be statically unstable. Equation 18 defines the relationship between the location of the neutral position with the AC location, the stabilizer efficiency (η_s), the slope of the main wing's lift curve (a_w), the slope of the stabilizer's lift curve (a_s), and the change in stabilizer downwash angle versus change in wing angle of attack ($\partial\varepsilon/\partial\alpha_s$).

$$x_n = x_w + \eta_s \frac{A_s(x_s - x_w)}{A_w \bar{c}} \cdot \frac{a_s}{a_w}\left(1 - \frac{\partial\varepsilon}{\partial\alpha_s}\right) \quad (18)$$

Values for the stabilizer efficiency and the change in stabilizer downwash angle versus change in wing angle of attack were chosen to be their typical values of 0.6 and 0.4 respectively. Using equations 16, 17 and 18 to determine the forward and aft CG limits, the flight package envelope was plotted in Figure 18 below.

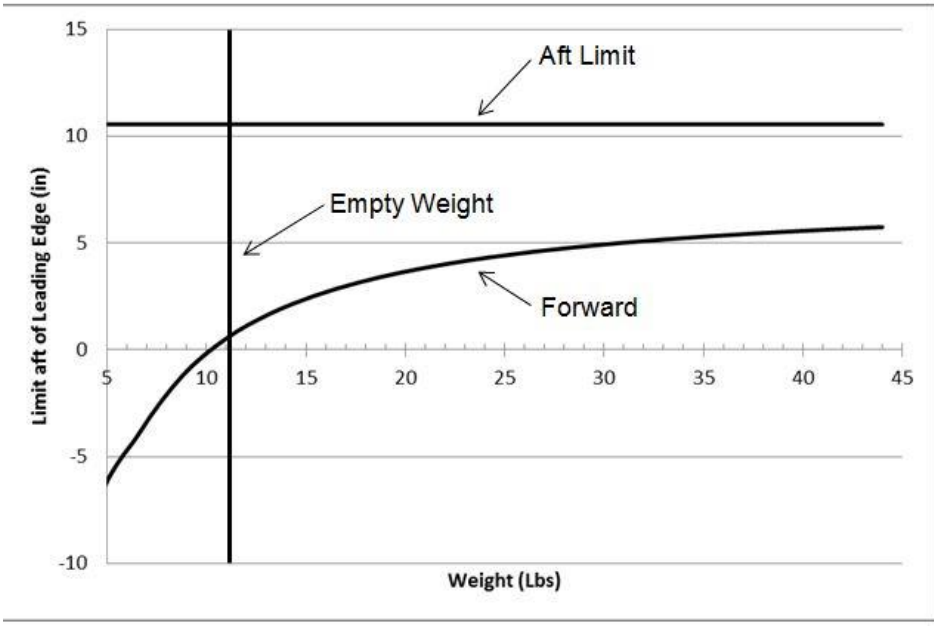

Figure 18: *The CG limit data plot used to find the aft and forward CG limits of the plane*

Table 1 calls out the appropriate CG limits for the fully unloaded plane of 11.2 lbs.

Table 1: *Displays the forward and aft CG limits for the empty aircraft, measured aft of the main wing's leading edge*

Empty Forward CG Limit (in)	0.5
Empty Aft CG Limit (in)	10.5

The dynamic longitudinal stability of the aircraft refers to its ability to return to level flight after an extended period of time. The analysis of this characteristic has to do with the distribution of the weight of the plane about the CG. A plane

with most of its mass centered about the CG or any of the extremities is likely to portray negative dynamic stability. This is caused by the concept of moment of inertia and the plane's axis of rotation. Due to the nature of this competition, most of the mass will be centered within the payload bay volume and within the main wing. It is for this reason that the plane will most likely not be dynamically stable. However, poor dynamic stability affects the plane's flight performance much less than poor static stability would. The pilot controlling the aircraft should be able to correct the flight trajectory with the remote controls fast enough to eliminate the issue.

4.0: CONCLUSION

The core objective of this project was to successfully design an aircraft, capable of lifting a maximum payload weight in stable flight, while abiding by all SAE rules and regulations. This year's team has worked towards a design best suited for competition by building and improving upon the strategies conducted by Union's previous teams. Major objectives that were defined to maintain a competitive design strategy consisted of abiding by all SAE rules and regulations, generating sufficient lift to carry the target payload weight, possessing the ability to maintain stable flight, and minimizing the unloaded weight of the plane.

The aircraft design for this year's plane utilizes a fully tapered wing with a 100 inch wingspan with an upright H-Tail stabilator design 38.5 inches aft of the main wing. The completion a full-scale fully-functioning prototype in the middle of the project's progression revealed many important design flaws that helped shape the final aircraft configuration. Had these issues not been addressed, the performance of this year's team would have been unfavorable. The final aircraft will weight 11.2 lbs. and be able to lift roughly 19 lbs., resulting in a payload fraction of 0.63.

Relevant research on the subject of induced drag and aerodynamic performance was compiled to help aid the efforts of future teams. A function that can be used to find any plane's allowable payload and corresponding takeoff velocity has been proven to be a useful tool. Additionally, information regarding induced drag and wing shape will deter future teams from a rectangular wing design and more towards a tapered design.

REFERENCES

[1] Corke, Thomas C. *Design of Aircraft*. Upper Saddle River, NJ: Prentice Hall, 2003. Print.

[2] Garner, W. B. *Model Airplane Propellers*. Tech. N.p.: n.p., 2009. Print.

[3] Jacobs, Eastman N., and Robert M. Pinkerton. *The Characteristics of 78 Related Airfoil Sections From Tests In The Variable-Density Wind Tunnel*. Tech. no. 460. N.p.: n.p., 1933. Print.

[4] Nicolai, Leland M. and Carichner, Grant, “Fundamentals of Aircraft and Airship Design, Volume I, Aircraft Design”, AIAA, Reston, Va, 2010

[5] Raymer, Daniel P. *Dan Raymer's Simplified Aircraft Design for Homebuilders*. Los Angeles, CA: Design Dimension, 2003. Print.

[6] Sadraey, Mohammad H. *Aircraft Design: A Systems Engineering Approach*. N.p.: n.p., n.d. Print.

[7] SAE Aero Rules Committee. "SAE Collegiate Design Series." *Rules*. N.p., n.d. Web. 06 Feb. 2014.

[8] Sartorius, Sky. "Oswald Efficiency Estimation Function." - *File Exchange*. N.p., n.d. Web. 01 Feb. 2014. <http://www.mathworks.com/matlabcentral/fileexchange/38800-oswald-efficiency-estimation-function>.

[9] "The Aerodynamic Center." *Aerostudents*. N.p., n.d. Web. <www.aerostudents.com>.

[10] "Web Analysis for Aerostudents." *Aerostudents : Aerostudents*. N.p., n.d. Web. 10 Nov. 2013.

[11] "UIUC Airfoil Data Site." *UIUC Airfoil Data Site*. N.p., n.d. Web. 21 Sept. 2013.

[12] "Longitudinal Static Stability." *Flying Qualities Phase*. Vol. 2. Edwards AFB: USAF Test Pilot School, 1990. N. pag. Print.

[13] *Elliptical Load Distribution on a Wing*. Digital image. *Remote Control Plane Website*. N.p., 24 June 2011. Web. 10 Mar. 2014. <http://aerospace.eng.usm.my/rcp/images/fea24.png>.

[14] *Pitch Roll and Yaw*. N.d. Photograph. *Night Time Level Design*. Web. 12 Mar. 2014. <http://bethbeinke.com/blog/2010/05/the-rotate-widget/>.

[15] "E423 (e423-il)." E423 (e423-il). University of Illinois, n.d. Web. 01 Mar. 2014. <airfoiltools.com>.

[16] Bouchard, Charles. *SAE Aero Design Team: Systems Engineering*. Tech. no. 1. Schenectady: Union College, 2012. Print

[17] Herzog, Adam, Nikolay Garabedian, Evan States, and Richard Hojnacki. *2014 SAE Aero Design East Design Report*. Rep. Schenctady: n.p., 2014. Print.

[18] Herzog, Adam. *SAE Aero Systems Engineer*. Poster. Schenctady: n.p., 2014. Print.

[19] Perkins, C.D., & Hage, R.E. (1949). *Airplane Stability and Control.* New York: John Wiley and Sons.